Mechanism of Alkaline Hydrolysis of Cyclic and Acyclic Sulfates: An ab Initio Study with Solvation Correction

Xabier Lopez,[†] Annick Dejaegere,*[,†,‡] and Martin Karplus*[,†,§]

Contribution from the Laboratoire de Chimie Biophysique, Institut le Bel, Université Louis Pasteur, 67000 Strasbourg, France, Groupe RMN−UPR 9003, ESBS Boulevard S. Brant, 67400 Illkirch, France, and Department of Chemistry & Chemical Biology, Harvard University, Cambridge, Massachusetts 02138

Received December 7, 1998. Revised Manuscript Received April 9, 1999

Abstract: The large difference in the activation barriers for the alkaline hydrolysis of cyclic and acyclic sulfate esters (the activation barrier of the cyclic sulfate is 10.3 kcal/mol lower than that for the acyclic sulfate, leading to 10^6-10^7-fold rate acceleration) is investigated. Ab initio studies of the reaction paths for the basic hydrolysis of ethylene sulfate (ES) and dimethyl sulfate (DMS) have been performed in vacuum and in solution. The calculations focus on the attack of the hydroxyl ion on sulfur, the rate-determining step for these reactions. In analogy with the calculated results for the isoelectronic phosphate esters (EP and DMP), differential solvation is the dominant factor that leads to the faster rate of hydrolysis of the cyclic ester. In both systems, the preferential solvation of the cyclic ester transition states is due primarily to the greater exposure and resulting stabilization of the attacking hydroxide ion. Although the differential solvation effects are the same, the overall effect of solvent is in opposite directions for the sulfate and the phosphate esters due to the fundamental difference in the electrostatic interactions involved (charge−charge for phosphates, charge−dipole for sulfates); i.e., the transition states for phosphate esters are stabilized by solvation, while they are destabilized for sulfate esters.

1. Introduction

Sulfate esters play an important role in vivo,[1−3] although they have been much less studied than their phosphate analogues.[4] The fact that sulfates have structures and hypervalent properties similar to those of phosphates may have important biological consequences. For example, Anderson et al.[5] have shown that phosphorylated analogues are good inhibitors of steroid sulfatases. How enzymes distinguish between sulfates and phosphates is also of interest.[1,2] More generally, there is the question of the relationship between the kinetics of the hydrolysis reactions of small sulfate and phosphate esters.[6,7] Of particular importance is the origin of the rate acceleration of the hydrolysis of the cyclic versus acyclic sulfate and phosphate esters. In the pioneering work of Westheimer,[8] it was shown that five-membered cyclic phosphates are hydrolyzed 10^6-10^8 times faster than acyclic phosphates, which corresponds to a difference in the free energy of activation of 10−12 kcal/mol. This difference had been ascribed for many years to ground-state destabilization arising from strain in the cyclic reactant.[8,9] However, recent theoretical studies[10−12] have demonstrated that most of the rate acceleration in the alkaline hydrolysis of cyclic ethylene phosphate (EP^-), relative to acyclic dimethyl phosphate (DMP^-), is due to differential solvation of the transition states. A corresponding role for solvent has been demonstrated for the base-catalyzed hydrolysis of methyl ethylene phosphate and nucleophilic attack on trimethyl phosphates.[13−15]

It is of particular interest to compare the rate acceleration in phosphate and sulfate esters because the overall effect of solvation on the reaction profile is expected to be qualitatively different. In phosphate ester hydrolysis by hydroxide, both reactants (EP^- or DMP^- and OH^-) have a charge of −1, and the transition state has a charge of −2. In vacuum, the two groups with a negative charge strongly repel each other, and the activation barrier is very large (on the order of 95 kcal/mol).[10,11] Since the solvation free energy varies with the square of the charge (e.g., in the Born model), one expects the transition states to be stabilized relative to the reactants. This is, in fact, what has been found in calculations; the transition-state barriers are lowered by about 60 kcal/mol in solution relative to those in the gas phase. For sulfate ester hydrolysis by hydroxide, the reactants are neutral dipoles (ethylene sulfate (ES) and dimethyl sulfate (DMS)) and an ion (OH^-). In such a situation, a stable ion−dipole complex is expected to be formed in the gas phase. However, when this system is solvated, the complex is expected to be significantly destabilized relative to reactants because the negative charge on the OH^- becomes distributed over a larger region in the transition state and a smaller Born stabilization, relative to the reactants, is expected.

* Corresponding authors. E-mail: A.D., annick@esbs.u-strasbg.fr; M.K., marci@tammy.harvard.edu.
† Université Louis Pasteur.
‡ Groupe RMN−UPR 9003.
§ Harvard University.

(1) Thatcher, G. R. J.; Cameron, D. R.; Nagelkerke, R.; Schmitke, J. *J. Chem. Soc., Chem. Commun.* **1992**, 382.
(2) Kanyo, Z. F.; Christianson, D. W. *J. Biol. Chem.* **1991**, *266*, 4264.
(3) Pflugrath, J. W.; Qiocho, F. A. *Nature* **1985**, *314*, 257.
(4) Westheimer, F. H. *Science* **1987**, *235*, 1173.
(5) Anderson, C. J.; Linda, J. H. L.; Widlanski, T. S. *J. Am. Chem. Soc.* **1995**, *117*, 3889.
(6) Kaiser, C. J.; Katz, I. R.; Wulfers, T. F. *J. Am. Chem. Soc.* **1965**, *87*, 3781.
(7) Kaiser, E. T. *Acc. Chem. Res.* **1970**, *3*, 145.
(8) Westheimer, F. H. *Acc. Chem. Res.* **1968**, *1*, 70.
(9) Kluger, R.; Taylor, S. D. *J. Am. Chem. Soc.* **1990**, *112*, 6669.
(10) Dejaegere, A.; Karplus, M. *J. Am. Chem. Soc.* **1993**, *115*, 5316.
(11) Dejaegere, A.; Liang, X.; Karplus, M. *J. Chem. Soc., Faraday Trans.* **1994**, *90*, 763.
(12) Cramer, C. J.; Hawkins, C. D.; Truhlar, D. G. *J. Chem. Soc., Faraday Trans.* **1994**, *90*, 1802−1804.
(13) Chang, N. Y.; Lim, C. *J. Am. Chem. Soc.* **1998**, *120*, 2156.
(14) Chang, N.; Lim, C. *J. Phys. Chem. A.* **1997**, *101*, 8706−8713.
(15) Florian, J.; Warshel, A. *J. Am. Chem. Soc.* **1997**, *119*, 5473.

10.1021/ja984193q CCC: $18.00
Published on Web 05/27/1999

To perform a detailed study of the alkaline hydrolysis of cyclic and acyclic sulfate esters and determine the origin of the difference between their activation barriers, we consider the transition states (as well as the intermediates) for the ES and DMS hydrolysis by ab initio techniques and compare their stabilities in vacuum and in solution. The various species are characterized structurally and energetically at a series of ab initio levels to verify the reliability of the results. The intermediates, but not the transition states, were studied by Thatcher and Cameron,[16] and we compare the present results with theirs where possible. For evaluating the effect of solvation, two methods are used. In the first, which is the same as that applied to the phosphate hydrolysis reaction,[10,11] the solvation of a given quantum-mechanically determined gas-phase structure and charge distribution was calculated by solving the linearized Poisson−Boltzmann equation.[17−20] In addition, we used the polarizable continuum model[21,22] (PCM), in which the quantum mechanical calculations are done in the presence of the solvation correction so that its effect on the structure and charge distribution can be determined.

2. Methods

2.1. Gas-Phase Calculations. Gaussian 94[23] was used for all ab initio calculations, except where stated. Structures were first optimized at the HF/3-21+G* level of theory with the Berny Newton−Raphson-type algorithm in Gaussian 94. Frequency calculations were made at the optimized geometries to verify that the structures were minima (positive Hessian matrix) or transition states (only one negative eigenvalue in the Hessian matrix). Single-point energy calculations at the MP2/6-31+G* level of theory were performed at these geometries. Starting from the HF/3-21+G* structures, the geometries were reoptimized at correlated levels of theory and with a larger basis set; both B3LYP/6-31+G* and MP2/6-31+G* were used. Vibrational frequencies were calculated at the B3LYP/6-31+G* geometries at the same level of theory; for the MP2/6-31+G* structures, no frequency calculations were done. At the B3LYP/6-31+G* geometries, single-point energy calculations at the B3LYP/6-311++G** level of theory were performed to check that a larger basis set with diffuse and polarization basis functions on the hydrogens did not change the description of the reaction.

The B3LYP/6-31+G* geometries and vibrational frequencies were used to evaluate thermodynamic parameters for the stationary points on the surface. The enthalpy was obtained as the sum of the B3LYP energy, the zero-point vibrational energy (ZPVE), the vibrational correction to the ZPVE at 298 K, the rotational and translational energies, and the $P\Delta V$ terms (determined as ΔnRT). The zero-point vibrational energy and the thermal vibrational energy were calculated in the rigid rotor−harmonic oscillator approximation.[24] The rotational and translational energies were treated classically as $^1/_2RT$ per degree of freedom.

To obtain physical insights into the results, the energies (relative to that of the reactants) associated with the various stationary points along the reaction profile were decomposed into deformation and interaction contributions; i.e., $\Delta E = \Delta E_{DEF} + \Delta E_{INT}$. The deformation energy, ΔE_{DEF}, for the cyclic ion−molecule complex (IMC), for example, is defined as

$$\Delta E_{DEF}(\mathrm{IMC}) = E[\mathrm{ES}]_{IMC} + E[\mathrm{OH}^-]_{IMC} - E[\mathrm{ES}] - E[\mathrm{OH}^-] \quad (1)$$

where $E[\mathrm{ES}]_{IMC}$ and $E[\mathrm{OH}^-]_{IMC}$ are single-point energies computed for the reactants ES and OH^- at the geometries that they assume in the ion−molecule complex and E(ES) and $E(OH^-)$ are the energies of the isolated ethylene sulfate and hydroxy anion. The deformation energy term is positive by definition and represents the cost of deforming the reactants to the conformation they adopt in the complex. The interaction energy, ΔE_{INT}, for the cyclic ion−molecule complex, for example, is defined as

$$\Delta E_{INT}(\mathrm{IMC}) = E[\mathrm{IMC}] - E[\mathrm{ES}]_{IMC} - E[\mathrm{OH}^-]_{IMC} \quad (2)$$

where E[IMC] is the total energy of the ion−molecule complex and $E[\mathrm{ES}]_{IMC}$ and $E[\mathrm{OH}^-]_{IMC}$ have the same definition as above. Corresponding equations were used for all stationary points along the profile. Given these results, the ring strain argument invoked to explain the difference in reactivity between the cyclic and acyclic compounds is equivalent to the requirement that the deformation energy of the acyclic complexes is greater than that of the cyclic ones. An alternative, more standard analysis of strain is based on a comparison of the heats of formation of an appropriate set of compounds.[10,25] We can write

$$E(\mathrm{strain}) = [E(\mathrm{ES}) - E(\mathrm{DMS})] - [E(\mathrm{TMS}) - E(\mathrm{MES})] \quad (3)$$

where TMS and MES stand for trimethylene and methylethyl sulfate, respectively. This method was employed by Thatcher and Cameron[16] to estimate the strain in the cyclic pentacovalent intermediate; they obtained a value of 4.6 kcal/mol.

2.2. Solvation Effect Calculations. 2.2.a. Poisson−Boltzmann Calculation. The effect of solvation for every stationary point on the potential surface was calculated by the finite difference linearized Poisson−Boltzmann continuum model,[17,18] which provides an accurate description of the solvation free energy for a given structure and charge distribution when electrostatic effects are dominant.[19,20] To define the dielectric boundary, the volume occupied by the solute was determined using a spherical probe with 1.4-Å radius (corresponding to a water molecule) rolling over the solute surface calculated from the van der Waals envelope. The Poisson−Boltzmann calculations were made with the UHBD program,[26] as modified for use with CHARMM by M. Schaefer (private communication). The radii (in Å) used to define the solute shape were as follow: sulfur, 2.015; sulfuryl oxygen, 1.70; ester oxygen, 1.77; carbon, 1.80; aliphatic proton, 1.468; hydroxyl oxygen, 1.796; and hydroxyl proton, 0.73. All values except that for sulfur are taken from the CHARMM 22 parameter set;[27] the sulfur radius, which is 2.15 Å in CHARMM, was taken from Thatcher and Cameron.[16] The values of the dielectric constants were set to 1 inside the cavity and 80 for the solvent. Two sets of geometries were employed: the B3LYP/6-31+G* geometries (referred as GAS) and the SCIPCM-B3LYP/6-31+G* (see below) geometries (referred as SCIPCM). For the atomic charges, the B3LYP/6-31+G* and SCIPCM-B3LYP/6-31+G* Mulliken charges were used.

2.2.b. Polarization Continuum Model. To determine changes in geometries and relative energies due to solvation, we used a combination of the self-consistent isodensity polarizable continuum model (SCI-

(16) Thatcher, G. R. J.; Cameron, D. L. *J. Chem. Soc., Perkin Trans. 2* **1996**, 767.
(17) Bashford, D.; Karplus, M. *Biochemistry* **1990**, *29*, 10219.
(18) Lim, C.; Bashford, D.; Karplus, M. *J. Phys. Chem.* **1991**, *95*, 5610.
(19) Arald, J. C.; Nicholls, A.; Sharp, K.; Honig, B.; Tempczyk, A.; Hendrickson, T. F.; Still, W. C. *J. Am. Chem. Soc.* **1991**, *113*, 1454.
(20) Mohan, V.; Davis, M. E.; McCammon, J. A.; Pettitt, B. M. *J. Phys. Chem.* **1992**, *96*, 6428.
(21) Tomassi, J.; Persico, J. *Chem. Rev.* **1994**, *94*, 2027.
(22) Wiberg, K. B.; Keith, T. A.; Frisch, M. J.; Murcko, M. *J. Phys. Chem.* **1995**, *99*, 9072.
(23) Frisch, M. J.; Trucks, G. W.; Schlegel, H. B.; Gill, P. M. W.; Johnson, B. G.; Robb, M. A.; Cheeseman, J. R.; Keith, T. A. P.; etersson, G. A.; Montgomery, J. A.; Raghavachari, K.; Al-Laham, M. A.; Zakrzewski, V. G.; Ortiz, J. V.; Foresman, J. B.; Peng, C. Y.; Ayala, P. A.; Wong, M. W.; Andres, J. L.; Replogle, E. S.; Gomperts, R.; Martin, R. L.; Fox, D. J.; Binkley, J. S.; Defrees, D. J.; Baker, J.; Stewart, J. P.; Head-Gordon, M.; Gonzalez, C.; Pople, J. A. *Gaussian 94*; Gaussian, Inc.: Pittsburgh, PA, 1995.
(24) Hehre, W. J.; Radom, L.; Schleyer, P. v. R.; Pople, J. A. *Ab Initio Molecular Orbital Theory*; Wiley-Interscience: New York, 1986.
(25) Allinger, N. A.; Tribble, M. T.; Miller, M. A.; Wertz, D. H. *J. Am. Chem. Soc.* **1971**, *93*, 1637.
(26) *Reviews in Computational Chemistry IV*; Lipkowitz, K. B., Boyd, D. B., Eds.; VCH Publishers: New York, 1993; pp 229−257.
(27) MacKerell, A. D., Jr.; Bashford, D.; Bellott, M.; Dunbrack, R. L., Jr.; Evanseck, J. D.; Field, M. J.; Fischer, S.; Gao, J.; Guo, H.; Ha, S.; Joseph-McCarthy, D.; L., K.; Kuczera, K.; Lau, F. T. K.; Mattos, C.; Michnick, S.; Ngo, T.; Nguyen, D. T.; Prodhom, B.; Reiher, W. E., III; Roux, B.; Schlenkirch, M.; Smith, J. C.; Stote, R.; Straub, J.; Watanabe, M.; Wiorkiewicz-Kuczera, J.; Yin, D.; Karplus, M. *J. Phys. Chem. B* **1998**, *102*, 3586−3616.

PCM)[22] and the PCM approaches.[21] Polarizable continuum models are based on a description of the solvent as a macroscopic continuum medium, as in the Poisson−Boltzmann calculations. The solute molecule is embedded in a cavity in the dielectric medium, and solute−solvent interactions are described by a reaction potential arising from the presence of the dielectric medium. In the original PCM, the polarization of the solvent is represented by a charge density introduced on the surface of the cavity surrounding the solute. The reaction potential $\Phi(r)$ at a point r takes the form

$$\Phi(r) = \int_S \mathrm{d}^2 r^t \frac{\sigma(r^t)}{|r - r^t|} \tag{4}$$

where S denotes the surface of the cavity and $\sigma(r^t)$ is the surface charge density at point r^t; it depends on the electric field exerted by the solute and the dielectric constant of the medium. The shape of the cavity is described in standard PCMs in terms of envelopes of spheres centered on atoms or atomic groups. The cost of these calculations is considerable because of the slow convergence of the numerical integrations used to determine $\Phi(r)$, largely due to the discontinuity of the potential at the intersection of the spheres. Moreover, these discontinuities often lead to noncontinuous gradients that create problems for geometry optimization; in fact, PCM geometry optimization calculations failed for our systems.

A number of improvements have been suggested to introduce more realistic cavities. One possibility is to define a cavity based upon an isosurface of the total electron density (SCI-PCM). The cavity is derived from the electronic density, which leads to a surface which is smooth and easily integrable. This reduces the computational cost and improves the geometry optimization procedure because discontinuities in the gradient are avoided. Geometry optimizations with the SCI-PCM level of theory were successful. These calculations were done using the B3LYP/6-31+G* method. They are referred to as the B3LYP(SCI-PCM)/6-31+G* level of theory in what follows.

However, for the present systems (and anions in general), the solvation energies obtained from the SCI-PCM are generally too low. For the extreme case of OH^-, the SCI-PCM solvation energy with the standard density contour value of 0.0004 au is −69 kcal/mol, as compared with the experimental estimate of −108 kcal/mol. The origin of the underestimation is the diffuseness of the electron density of anions, which leads to isodensity surfaces that are too large. Thus, although SCI-PCM can give a qualitative description of the solvent effect on geometries and charge polarization, more quantitative results require use of a smaller cavity or very extensive reparametrization.[28] By contrast, the PCM with the cavity defined by spheres that are 1.2 times the van der Waals radii[29] yields satisfactory solvation free energies; for the hydroxyl anion, for example, the value is −97 kcal/mol, in much better agreement with the experimental estimate.

To overcome the two types of problems (difficulty of optimization, incorrect anion solvation), we used a combination of the SCI-PCM and PCM methods. The geometries were optimized with the SCI-PCM method at the B3LYP/6-31+G* level, and the solvation free energies for the SCI-PCM stationary points were recalculated with the PCM method using the van der Waals cavity described above. For these PCM calculations, we used the HF/6-31+G* level of theory and the GAMESS program.[30] The solvation free energy (G_{solv}) is estimated in this combined approach from the difference between the HF(PCM)/6-31+G* energy for the SCI-PCM geometry and the HF/6-31+G* energy for the gas-phase B3LYP/6-31+G* geometry.

The barriers in aqueous solution ($\Delta G^{\ddagger}_{aq}$) are then estimated by adding the solvent contribution ($\Delta G^{\ddagger}_{solv}$) to the gas-phase barrier (ΔG_{gas}), calculated at B3LYP/6-31+G*. $\Delta G^{\ddagger}_{solv}$ is defined as the difference in solvation free energies between reactants and the transition state ($\Delta G^{\ddagger}_{solv} = G^{TS}_{solv} - G^{R}_{solv}$), both calculated by the hybrid approach described above.This theoretical level will be referred to as PCM. The solvation free energies (G_{solv}) and relative Gibbs free energies in solution ($\Delta G^{\ddagger}_{aq}$) can be found in Table 3.

3. Results and Discussion

The gas-phase reaction profiles for the sulfates are presented in section 3.1, and the results for the solvated systems are described in section 3.2. A comparison with phosphate ester hydrolysis is made in section 4.

3.1. Gas-Phase Structures and Reaction Profiles. 3.1.a. Structures. Three different types of gas-phase stationary points were found for both the cyclic and the acyclic sulfates. There is a long-range bidentate ion−molecule complex (IMC for the cyclic, IMAC for the acyclic); there is the transition state corresponding to the attack of OH^- on the sulfur (TSC for the cyclic, TSAC for the acyclic); and there are stable pentacovalent intermediates (one in the cyclic case, IC, and three for the acyclic case, IAC, IAC′, IAC″). The geometries and energies of the reactants (ES for the cyclic and DMS for the acyclic reaction, as well as that of OH^-) were also determined. The geometries of the gas-phase stationary points are given in Figure 1a for the cyclic sulfates and in Figure 1b for the acyclic sulfates; values for three levels of theory are reported (see section 2.1). Table 1a lists a more complete set of structural parameters from the gas-phase calculations at the B3LYP/6-31+G* level. Comparison of the results at different levels of theory shows that they are generally similar but that there are nonnegligible differences. For most of the geometric parameters, the B3LYP/6-31+G* and MP2/6-31+G* values are in good agreement, with the HF/3-21+G* values showing larger differences. The HCCH dihedral angle of the cyclic esters, in particular, is quite variable (up to 8°) and does not show consistent convergence.

The first step in the nucleophilic attack by OH^- is the formation of an ion−molecule complex, in agreement with what has been observed for other gas-phase nucleophilic attacks on a neutral reactant.[31] It can be seen that the hydroxyl ion forms a bidentate complex, interacting with both aliphatic carbon groups of the reactants. In attempts to find a monodentate complex, optimizations at the HF/3-21+G* level of theory were started from structures in which the hydroxyl oxygen was bound to an aliphatic hydrogen at a distance of 1.640 Å, and the force constants were computed at every point to determine if a minimum had been found. In all cases, the system collapsed into the bidendate complex. The overall geometries of the cyclic and acyclic ion−molecule complexes are very similar, except that hydroxyl oxygen distance to the methyl hydrogens of the acyclic complex is significantly shorter than the corresponding distance in the cyclic compound due to geometric constraints in the latter. The geometry of the cyclic ion−molecule complex is slightly distorted relative to the reactant ES by the presence of the OH^-; e.g., the C−C and S−O bonds are shortened and the C−O bonds elongated with respect to ES. Also, because the OH^- binding is somewhat asymmetric, a corresponding asymmetry is induced in ES. Deformations are observed also for IMAC, although the complex is more symmetric. In the acyclic complex there are larger changes in certain bond angles than in the cyclic compound (see Table 1a), as shown by a comparison of $O_{ap}-S-O_{eq}$ and $S-O_{ap}-C$, for example.

The transition states TSC and TSAC have very different geometries from the ion−molecule complex. As can be seen in Figure 1a, the OH^- has moved a long distance to bring it into position for apical attack on the sulfur. To examine the nature of the "intramolecular" path, additional calculations were

(28) Barone, V.; Cossi, M.; Tomasi, J. *J. Chem. Phys.* **1997**, *107*, 3210.
(29) Cossi, M.; Barone, V.; Cammi, R.; Tomasi, J. *Chem. Phys. Lett.* **1996**, *255*, 327−335.
(30) GAMESS: Schmidt, M. W.; Baldridge, K. K.; Boatz, J. A.; Elbert, S. T.; M. S. Gordon, J.; Jensen, J.; Koseki, S.; Matsunaga, N.; Nguyen, K. A.; Su, S.; Windus, T. L.; Dupuis, M.; Montgomery, J. A. *J. Comput. Chem.* **1993**, *14*, 1347−1363.
(31) Braumann, X. X. *Science* **1998**, *279*, 1892.

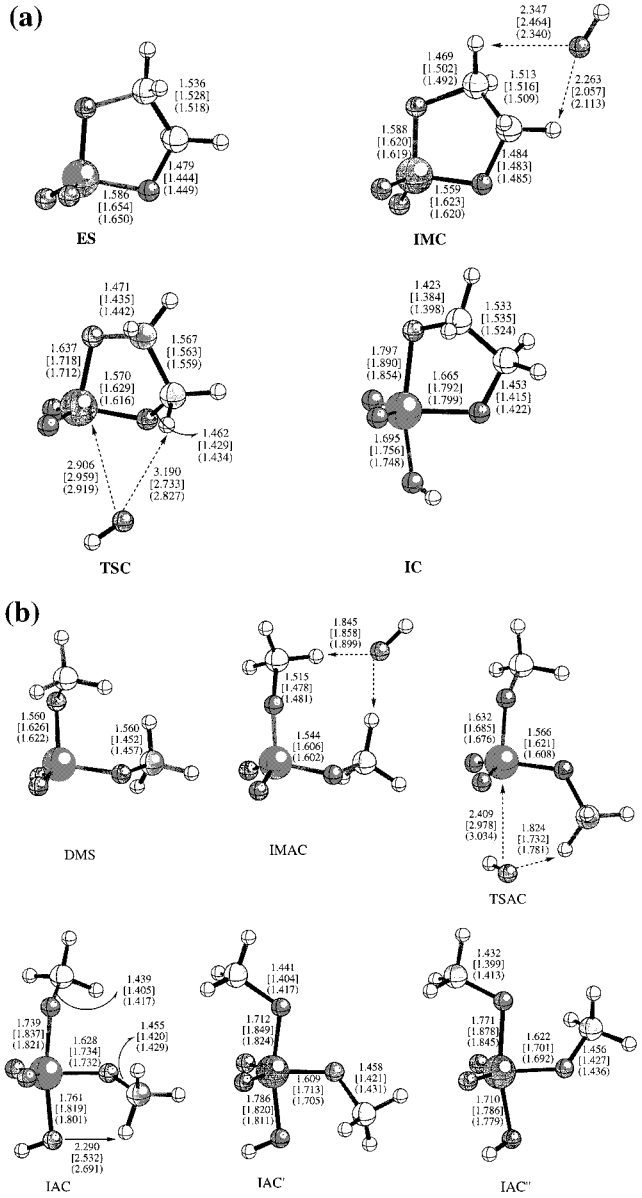

Figure 1. (a) Optimized geometries of the local minima and transition states of the $[ES-OH]^-$ gas-phase potential surface. Results correspond to calculations with HF/3-21+G*, B3LYP/6-31+G* (in brackets), and MP2/6-31+G* (in parentheses). All distances are in angstroms. (b) Optimized geometries of the local minima and transition states of the $[DMS-OH]^-$ gas-phase potential surface. Results correspond to calculations with HF/3-21+G*, B3LYP/6-31+G* (in brackets), and MP2/6-31+G* (in parentheses). All distances are in angstroms.

performed. In the cyclic case, the intrinsic reaction coordinate[32,33] (IRC) was followed with the B3LYP/6-31+G* method, starting from the transition state (Figure 2a). The calculation include S- - -OH distances between 1.796 Å on the right of the figure (intermediate-like, see Figure 1a) and 4.175 Å on the left of the figure. Starting with the intermediate, the hydroxyl moiety moves away from the sulfur atom in the direction of the bidentate complex. In the transition state, the hydroxyl moiety is situated approximately equidistant from the S atom and one of the aliphatic hydrogens. It then approaches one of the aliphatic hydrogens and comes significantly closer to it than in the transition state. The last point shown in Figure 2a has an energy that is 10 kcal/mol higher than that of the bidentate complex and is not a local minimum. Since such IRC calculations are very slow, the rest of the path was investigated by departing from the "monodentate" structure and using a simplified procedure to find a path to the bidendate structure (Figure 2b). First, a constrained geometry optimization was performed with the (C)H- - -O(H) distance (i.e., the distance between the aliphatic hydrogen and the oxygen of the attacking OH) fixed at 1.610 Å, obtained for the last point in Figure 2a. From this structure (the first geometry depicted in Figure 2b), a geometry optimization with no constraints was performed. The result was that the system collapsed to the bidentate species. The structures in Figure 2b correspond to geometries along the "collapse" path. As can be seen, the OH group moves around the nearest methylene hydrogen with increasing methylene hydrogen−hydroxyl oxygen distance until it reaches the bidentate ion complex structure. Although this is not an IRC path, it gives qualitative information concerning the large structural changes involved in the reaction.

A corresponding minimization analysis was made for the acyclic system to determine the path between the bidentate complex and transition state. Figure 2c shows the starting structure, which is close to TSAC, and several structures obtained during the minimization. Attempts to obtain a monodentate ion−molecule complex with a geometry more similar to the TSAC always resulted in the bidentate complex. It can be seen that the OCH_3 group with which the OH^- interacts rotates with it and facilitates the transition to the bidentate ion−molecule complex. To test whether the results were due to a limitation of the basis set, optimizations were redone using a higher level (i.e., 6-31++G**); the structures followed a similar pathway and collapsed to the bidentate complex as before.

The interesting and rather complex "intramolecular" path between the initial bidentate ion−molecule complex and the transition state for the reaction in both the cyclic and acyclic systems appears to involve a monotonic increase in energy toward the transition state without any monodentate intermediates. If they were to exist, though we were not able to find them, they would have to be much less stable than the bidentate complexes and represent shallow local minima on the potential energy surface with a low barrier toward the collapse to the bidentate structure. Thus, they would not be kinetically relevant.

The cyclic and acyclic transition states (TSC and TSAC, respectively) are shown in Figure 1; see Table 1a for details of the structures. An important aspect of both of the transition-state structures is the long-range (early) nature of the transition states; i.e., the bond between the sulfur and the attacking O of the OH^- is very long (2.9 Å), and the bond between the apical O (leaving group) and S is only slightly elongated (0.1 Å), relative to the reactant values of 1.6 Å. For TSAC, there is a large difference in the S- - -O(H) distances calculated with (2.9 Å) and without (2.4 Å) electron correlation; the B3LYP and MP2 structures are in good agreement.

As can be seen by comparing with the intermediate structures that occur after the transition state, the reaction is concerted in that one bond is formed while the other is elongated. This is similar to the behavior observed in the alkaline hydrolysis of phosphate esters.[11] In ethylene phosphate, the P- - -OH distance is somewhat shorter (i.e., in EP- - -OH, P- - -OH is 2.6 Å) and the $P-O_{ax}$ bonds are somewhat longer (i.e., in EP- - -OH, P- - -O_{ax} is 1.86 Å). This is in accord with the concept of a concerted mechanism, in that as the OH approaches, the $X-O_{ax}$ bond is elongated, with X = P or S. These results do not fit directly into the dissociative/associative classification that is often used

(32) Gonzalez, C.; Schlegel, B. *J. Chem. Phys.* **1989**, *90*, 2154.
(33) Gonzalez, C.; Schlegel, H. B. *J. Phys. Chem.* **1990**, *94*, 5523.

Table 1. Geometries of Stationary Points for the Cyclic and Acyclic Sulfate Hydrolysis in the Gas Phase[a,b] (a) and for the Cyclic and Acyclic Sulfates with Solvation Correction[a,c]

(a) Cyclic and Acyclic Sulfate Hydrolysis in the Gas Phase

	reactants		ion−molecule		transition state		intermediate	
	cyclic	acyclic	cyclic	acyclic	cyclic	acyclic	cyclic	acyclic
S−OH	–	–	–	–	2.959	2.978	1.756	1.819
S−O_{ap}	1.654	1.626	1.623	1.606	1.718	1.685	1.890	1.837
S−O_{eq}	1.654	1.626	1.620	1.606	1.629	1.621	1.792	1.734
C−O_{ap}	1.450	1.452	1.484	1.478	1.435	1.428	1.405	1.405
C−O_{eq}	1.450	1.452	1.502	1.478	1.429	1.470	1.420	1.420
C−C	1.528	–	1.516	–	1.563	–	1.535	–
O_{ap}−S−O_{eq}	95.31	101.78	97.03	105.92	89.44	94.42	83.91	85.77
S−O_{ap}−C	110.12	116.95	110.00	120.09	107.00	116.58	108.42	117.10
S−O_{eq}−C	110.12	116.95	110.94	120.09	106.06	118.73	115.87	113.22
O_{ap}−C−C	104.28	–	104.32	–	106.78	–	104.51	–
O_{eq}−C−C	104.28	–	104.32	–	104.31	–	107.10	–
C−O_{ap}−S−O_{eq}	13.10	74.96	17.81	82.41	39.51	68.77	35.02	67.62
C−O_{eq}−S−O_{ap}	13.10	74.96	5.42	82.41	49.58	138.72	11.17	97.74
O_{ap}−C−C−O_{eq}	41.00	–	36.36	–	14.39	–	38.41	–
H−C−C−H	38.50	–	35.58	–	12.72	–	36.00	–
O_{eq}(C)−S−O(H)			45.46	59.38	61.45	78.29	82.00	86.24
O_{ap}−S−O(H)			51.59	59.38	138.70	172.65	164.68	170.78
C−O_{eq}−S−O(H)			18.34	−44.08	18.34	−42.11	−174.89	−77.66

(b) Cyclic and Acyclic Sulfates with Solvation Correction

	reactants		transition state		intermediate	
	cyclic	acyclic	cyclic	acyclic	cyclic	acyclic
S−OH	–		3.117	2.635	1.761	1.813
S−O_{ap}	1.633	1.613	1.670	1.678	1.851	1.822
S−O_{eq}	1.633	1.613	1.642	1.626	1.749	1.712
C−O_{ap}	1.462	1.463	1.445	1.439	1.399	1.414
C−O_{eq}	1.462	1.463	1.460	1.458	1.431	1.430
C−C	1.525	–	1.522	–	1.529	–
O_{ap}−S−O_{eq}	96.43	103.17	94.59	98.64	85.09	86.82
S−O_{ap}−C	110.12	117.83	110.06	117.50	108.91	117.51
S−O_{eq}−C	110.12	117.83	111.30	117.90	116.21	114.58
O_{ap}−C−C	104.13	–	103.68	–	104.12	–
O_{eq}−C−C	104.13	–	104.62	–	106.38	–
C−O_{ap}−S−O_{eq}	12.69	70.23	17.95	86.27	34.20	63.39
C−O_{eq}−S−O_{ap}	12.69	70.23	7.83	121.07	10.69	89.74
O_{ap}−C−C−O_{eq}	39.62	–	40.26	–	37.36	–
H−C−C−H	37.22	–	16.74	–	34.63	–
O_{eq}(C)−S−O(H)			68.46	79.89	82.50	86.24
O_{ap}−S−O(H)			162.84	174.48	166.16	170.78
C−O_{eq}−S−O(H)			169.50	−56.66	−175.44	−77.66

[a] Values are calculated at the B3LYP/6-31+G* level. All distances are in angstroms and angles in degrees. For the acyclic system, only the data for the IAC intermediate are shown. [b] The calculated O−H bond length is 0.975 Å. [c] The calculated O−H bond length is 0.972 Å.

for discussing phosphate (and sulfate) ester hydrolysis,[34] where one expects both bonds at the transition state to be near their equilibrium values (associative) or significantly longer (dissociative).

Both TSC and TSAC are stabilized by interactions between the OH^- moiety and one of the aliphatic hydrogens. In the acyclic case, an equatorial methoxy group rotates to bring it closer to the hydroxyl ion; the hydroxy−methoxy distance (O(hydroxyl)−H(CH_3)) is only 1.732 Å with B3LYP. In the cyclic case, the dihedral angle constraints on the methylene groups prevent such a rotation, and it is the OH^- moiety which moves toward the aliphatic hydrogens. Since the OH^- cannot move too far from the sulfur, the O(hydroxyl)−H(CH_2) distance is much longer (2.73 Å) in the cyclic than in the acyclic transition state. Figure 1b for the DMS reaction, as well as the values presented in Table 1a, shows that the C−O_{eq}−S−O_{ap} dihedral angle rotates from gauche (∼75°) in the acyclic reactant and ion−molecule complex to a conformation approaching the trans region (138.7°) in the transition state. This conformational flexibility does not exist in the cyclic reactant.

(34) Admiraal, S. J.; Herschlag, D. *Chem. Biol.* **1995**, *2*, 729.

Pentacovalent intermediates are formed after the transition states for both the cyclic and acyclic reactions; the geometry of IC is shown in Figure 1a, and those of IAC, IAC′, and IAC″ are shown in Figure 1b. A comparison of the bond distances and angles for the cyclic and acyclic stationary points and reactants is given in Table 1a. As already mentioned, the elongation of the S−O leaving group bond has continued relative to the TS in both systems. However, it is of interest to note that the conformation of the ring in IC is more similar to that of the reactant than to the transition state; i.e., in both IC and ES, the aliphatic hydrogens are in a staggered conformation, whereas they are eclipsed in TSC. The O_{ap}−S−O_{eq} angle internal to the ES ring is 6.5° smaller than the corresponding angle in the acyclic DMS (95.3° vs 101.8°), in agreement with Thatcher and Cameron.[16] This difference is accentuated in the ion−molecule complex (97.0° vs 105.9°) and only slightly reduced in the transition state (89.4° vs 94.4°). In the intermediates, on the other end, this angle is similar for both systems (83.9° for IC and 85.8° for IAC). The S−O_{eq}−C angles are very different from the transition-state values; in IC it is larger by 10°, and in IAC it is smaller by 5.5°. The S−O_{ap} and S−O_{eq}

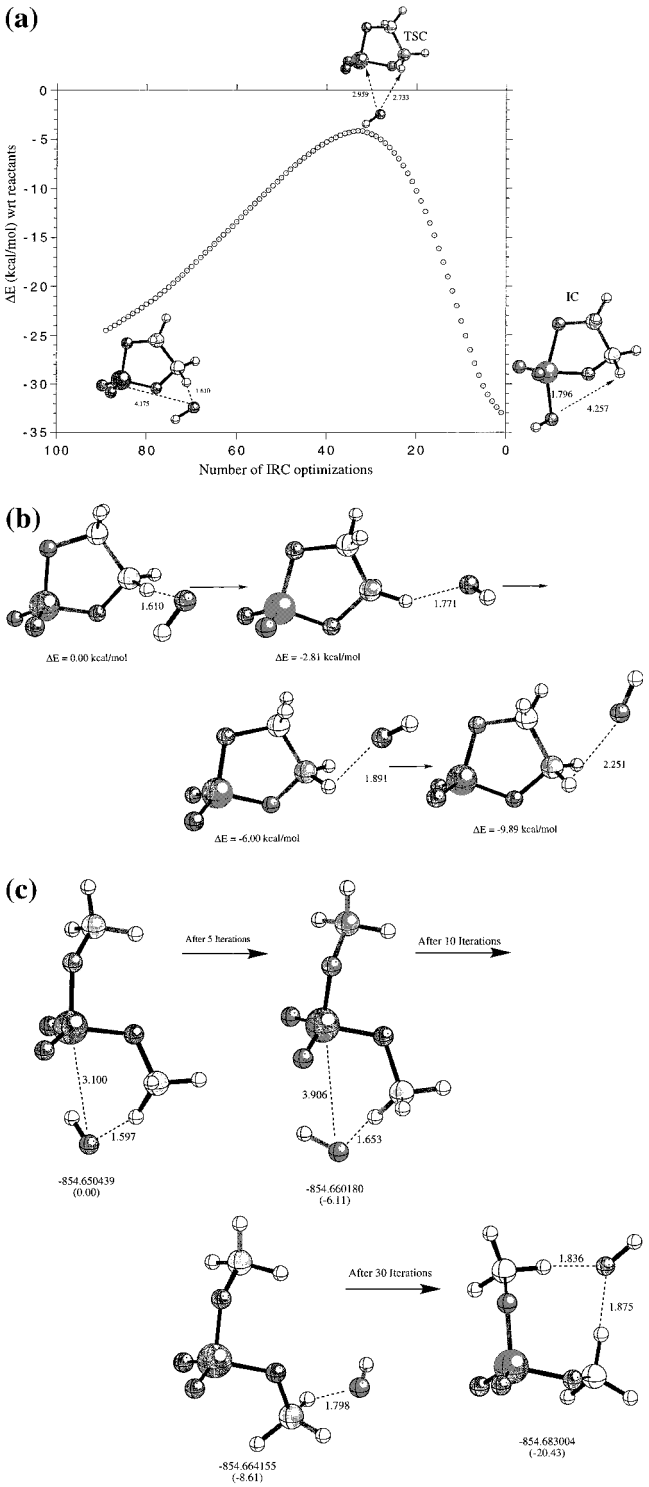

Figure 2. (a) B3LYP/6-31+G* IRC calculation starting from the cyclic transition state. The two final structures and the TSC geometry are shown with the S−O(H) and CH- -OH distances in angstroms. (b) Structures along the search of a monodentate ES−OH ion−molecule complex at the B3LYP/6-31+G* level of theory. From the last IRC structure, a partial geometry optimization of a monodentate ES−OH complex was done, constraining the (C)H- - -OH distance to 1.610 Å (first structure of the figure). From that structure, a full geometry optimization was performed. The structure collapsed to the bidentate ion−molecule complex. In the figure, we depict some of the structures observed along the full geometry optimization. The relative energies, in kcal/mol, with respect to the initial geometry are also reported. (c) Structures along the B3LYP/6-31+G* optimization of [DMS−OH]$^-$ to determine the path from the transition state to the bidentate ion−molecule complex (see text).

Table 2. (a) Gas-Phase Relative Energies (Δ*E*), with Respect to the Reactants, Calculated at MP2/6-31+G*//HF/3-21+G* (MP2//HF), B3LYP/6-31+G* (B3LYP), B3LYP/6-311++G**//B3LYP/6-31+G* (B3LYP/BIG), and MP2/6-31+G* (MP2) Levels[a] and (b) Deformation Analysis, Listing Interaction Energies, in kcal/mol, for Cyclic and Acyclic Sulfates and the Deformation Energy for the Sulfate Moiety[b]

(a) Gas-Phase Relative Energies

structure	MP2//HF	B3LYP/BIG	MP2	B3LYP	Δ*H*	Δ*S*	Δ*G*
			Cyclic				
IMC	−36.6	−36.2	−37.3	−35.6	−35.6	−24.9	−28.2
TSC	−5.7	−4.5	−5.6	−4.1	−4.6	−31.4	4.8
IC	−39.9	−38.9	−41.0	−39.9	−39.3	−34.5	−29.0
			Acyclic				
IMAC	−30.9	−32.4	−30.8	−31.2	−31.4	−28.7	−22.8
TSAC	−14.7	−15.4	−14.0	−13.9	−14.9	−31.5	−5.5
IAC	−24.5	−25.1	−26.7	−26.1	−25.7	−32.2	−16.1
IAC′	−24.6		−25.8	−25.7	−25.3	−31.5	−15.9
IAC″	−25.3		−25.9	−25.5	−25.1	−31.9	−15.6

(b) Deformation Analysis

cyclic			acyclic		
compd	E_{INT}	E_{def}	compd	E_{INT}	E_{def}
IMC	−38.3	2.7	IMAC	−36.5	5.3
TSC	−12.8	8.6	TSAC	−22.9	9.0
IC	−92.2	52.1	IAC	−83.2	57.7

[a] Also reported are the Δ*H*, Δ*S*, and Δ*G* values calculated using the B3LYP/6-31+G* data. All quantitaties are given in kcal/mol, except for Δ*S* (cal mol^{-1} K^{-1}). ES+OH− total energies in au are −851.43235 (MP2/HF), −853.57612 (B3/BIG), −850.51346 (MP2), and −853.42334 (B3LYP); DMS+OH− total energies are −852.89901 (MP2/HF), −854.79085 (B3/BIG), −852.82990 (MP2), and −854.63434 (B3LYP). [b] Deformation values for OH$^-$ are not shown since all are below 0.015 kcal/mol. All energetics are calculated at the B3LYP/6-31+G* level of theory. A more detailed table with the total energies used for this deformation analysis is available in the Supporting Information.

bond distances are longer by 0.02−0.09 Å for the cyclic system than for the acyclic system at all stationary points. This is likely to be due to the geometrical constraints imposed by the ring in the cyclic sulfate, which do not allow the optimum (shorter) S−O bond length to be reached; i.e., a shorter S−O distance would require elongation of the CC bond and would lead to destabilization of the ring. The distances for the CC bond (1.528 and 1.535 Å, respectively) are similar in ES and IC; the latter value is very close to that in ethane (1.532 Å). The newly formed S−OH bond is shorter by 0.6 Å for the cyclic intermediate than for any of the acyclic intermediates.

3.1.b. Energetics. The gas-phase energies and free energies of the various species relative to the reactants are given in Table 2a from the calculations at the MP2/6-31+G*//HF/3-21+G*, B3LYP/6-31+G*, B3LYP/6-311++G**//B3LYP/6-31+G*, and MP2/6-31+G* levels of theory, while Table 2b lists the deformation energies relative to the reactants at the various levels. Although the absolute energies obtained with the different theoretical levels and basis sets used in this work are significantly different (see footnote to Table 2a), as expected, the relative energies are very similar; they vary by at most 2.1 kcal/mol for the cyclic intermediate (IC) comparing B3LYP/6-311++G** with MP2/6-31+G*. Such differences are unimportant for the mechanistic considerations of this paper. It is clear that the free energy is dominated by the energy differences. The vibrational corrections to the enthalpy are very small in all cases (between 0 and 1 kcal/mol), and the entropic contributions are small but not negligible. They vary from 7.4 to 9.5 kcal/mol at 300 K. A diagram comparing the gas-phase free energy profile of the cyclic and the acyclic reactions is presented in Figure 3.

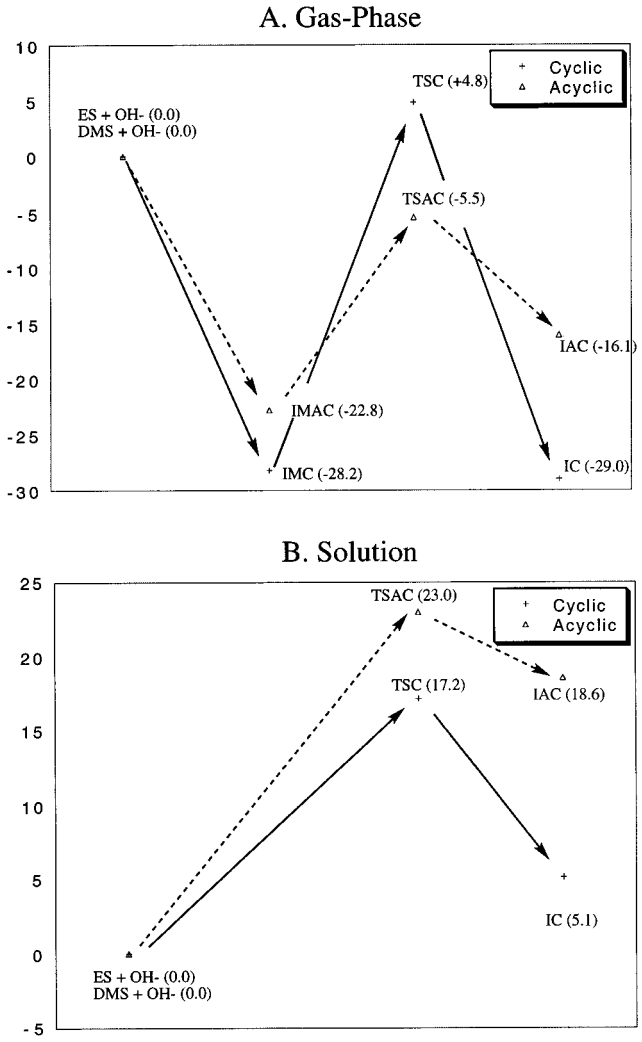

Figure 3. Free-energy diagrams for the hydrolysis of cyclic and acyclic sulfates, in the gas-phase at B3LYP/6-31+G* (A) and in solution at the PCM//SCIPCM level of theory (B) (see text). Energies are in kcal/mol.

As described in section 3.1.a, the first step of the gas-phase reaction is the formation of long-range ion−molecule complexes, which are significantly more stable than the reactants (ΔG_{gas}, relative to the reactants, equal to −28.2 and −22.8 kcal/mol for IMC and IMAC, respectively). The formation of the cyclic complex is thus more favorable than formation of the acyclic complex by 5.4 kcal/mol. From Table 2b, 4.2 kcal/mol of that stabilization arises from a more favorable enthalpy and 1.2 kcal/mol from a more favorable entropy. The entropy loss for the ion−molecule complexes is significantly less than that of the transition states. The results of the decomposition analysis for the energy (Table 2b and section 2.1) indicate that the cost of deforming the reactants to their geometry in the ion−molecule complex is larger for DMS than for ES and that the interaction energy is slightly more favorable in the cyclic complex, due to the larger dipole moment of ES.

The reaction then proceeds to the transition states (TSC and TSAC). It can be seen from Table 2a that the difference in energy between the reactants and the transition state is negative for the cyclic and the acyclic sulfates at all levels of theory; there are no energy barriers relative to the reactants in the gas phase at 0 K. When enthalpic and entropic contributions are included (see ΔG_{gas} in Table 2a), a barrier of 4.8 kcal/mol is obtained for the cyclic compound, while the acyclic transition state remains lower in free energy than the reactants by 5.5 kcal/mol. This results from the fact that, while the entropic contributions at the transition state are essentially the same, the energetic stabilization of the acyclic TS is significantly larger (by 10.3 kcal/mol) than that of the cyclic TS. The greater stabilization of the acyclic TS is due to the stronger (H)O- - -H(C) interaction between the incoming OH^- group and a methyl CH bond (see also below). Since the reaction is expected to proceed via the ion−dipole complex, the free energy barriers relative to it are important; they are 33 and 17.3 kcal/mol for the cyclic and acyclic sulfates, respectively. The decomposition analysis (Table 2b) shows that the deformation energy is similar for the cyclic and acyclic compounds in the transition state, in contrast to what is found in the ion−molecule complex. There is no evidence for relief of ring strain that stabilizes the cyclic transition state. This is in accord with the fact that the O−S−O angle internal to the ring (O_{ap}−S−O_{eq}) is still 5° smaller for the cyclic than for the acyclic compound.

The dominant contribution to the extra stability of the acyclic transition state arises, as mentioned above, from the presence of an interaction between the hydroxy oxygen and the aliphatic hydrogens of the equatorial methyl group of the sulfate. The hydroxyl oxygen in TSAC (Figure 1b) is at a distance of 1.732 Å (at B3LYP/6-31+G*) from one of the hydrogens of this methyl group, and the O(hydroxyl)−H(methyl)−C(methyl) angle is equal to 149.3°. Natural bond orbital calculations confirmed the strong interactions between lone pairs n_O of O(H) and antibonding σ^*_{C-H} orbitals. The $n_O \rightarrow \sigma^*_{C-H}$ interaction is determined in NBO analysis[35] by a second-order perturbation term of the form $-2\langle n_O|F|\sigma^*_{C-H}\rangle/(\epsilon n_o - \epsilon\sigma^*)$. For this case, we found two interactions of this type with values of −18 and −11 kcal/mol, respectively. To more precisely estimate the contribution of such interactions, we calculated the interaction energy between a hydroxy anion and a methanol molecule with the same relative orientation as the hydroxy and methoxy moieties in TSAC. The interaction energy is −11 kcal/mol. This is in good agreement with the stabilization of TSAC versus TSC. The strength of this CH- - -OH hydrogen bond has its origin in the large negative charge on the hydroxy oxygen, which can be stabilized by partial delocalization of its lone pairs into antibonding σ^*_{C-H} orbitals of methanol. This interaction is not present in the cyclic transition state, where the absence of rotational freedom with respect to the S−O bond leads to much longer distances (2.7 Å) between the hydroxy oxygen and the aliphatic hydrogens.

As already mentioned, there is one intermediate after the transition state for the cyclic sulfate, and there are three for the acyclic sulfate (Figure 1b). The three acyclic intermediates have nearly equal energies and free energies. In contrast to the transitions states, the cyclic intermediate is much more stable than the acyclic intermediates. This is in accord with the results of Thatcher and Cameron,[16] who reported on the IC, IAC′, and IAC″ intermediates. The energy difference between IC and IAC, IAC′, and IAC″ is about −14 kcal/mol, and this difference is maintained in the free energy (−12.9 kcal/mol). The entropy loss of the acyclic intermediates is slightly greater than that for the cyclic intermediate. The decomposition analysis of Table 2b shows that both terms (E_{INT} and E_{DEF}) are large because of the strong interactions in these intermediates relative to the reactants, so that the results must be interpreted with caution. The deformation energy of the cyclic compound is 5.6 kcal/mol less than that of the acyclic one. This is in accord with the fact that the O−S−O angle internal to the ring is 83.9° for the

(35) Reed, A. E.; Curtiss, L. A.; Weinhold, F. *Chem. Rev.* **1988**, *88*, 899.

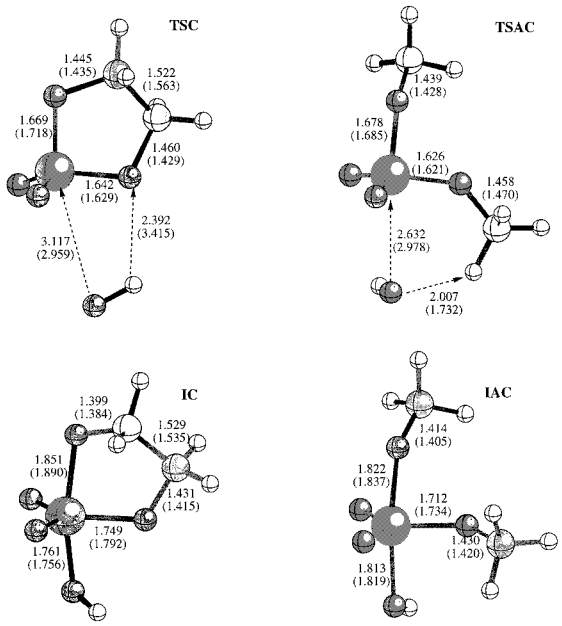

Figure 4. B3LYP(SCI-PCM)/6-31+G* geometries for the TSC, TSAC, IC, and IAC in solution. The corresponding gas-phase values are given in parentheses. All distances are in angstroms.

IC vs 85.8° for IAC′. This difference agrees with an estimate of the strain enthalpy of 4.6 kcal/mol based on eq 4. Thus, the results indicate that, of the 15 kcal/mol increased stability of IC versus IAC, about 5 kcal/mol results from the relief of ring strain. The remaining ~10 kcal/mol increased stability of the cyclic intermediate arises primarily from the difference in the interaction energy. The source of the latter is not clear. The hydrogen bond interactions stabilizing the acyclic transition state with respect to the cyclic one are not present in the acyclic intermediate; the distance between the incoming hydroxyl group and the aliphatic hydrogen is larger than 2.5 Å. Since the overlap between orbitals decays exponentially with the distance, the $n_O \rightarrow \sigma^*_{CH}$ delocalization is negligible in this case.

As our focus is on the rate-determining step of the reaction, we did not try to identify stationary points beyond the intermediates along the reaction path. For the cyclic system, they have been shown by Cameron and Thatcher[36] to include the transition state corresponding to the breaking of the S−O apical bond and the one corresponding to the pseudorotation process. These transition states involve lower barriers than those for the TS for the hydroxy attack on the sulfur.

3.2. Solvated Reaction Profile. There is an important change in the reaction path on solvation because of the change in the energetics. It is useful to describe first the solution structures along that path and then the energetics associated with it. The major difference is that the ion−molecule complex, which is very stable in the gas-phase, is at most a shallow minimum in solution, so that there is a direct attack of the OH^- group on the sulfur atom.

3.2.a. Structures. Starting with the gas-phase structures, the reactants, transition states, and pentacovalent intermediates were reoptimized to determine the changes in structure and charge distribution that result from solvation (see section 2.2). The geometric parameters are given in Table 1b; Figure 4 shows the structures of the transition states and intermediates for the reaction of ES and DMS with OH^-. The reactants and the pentacovalent intermediates IC and IAC are not much affected by solvation; the changes in the bond lengths are in the range 0.01−0.05 Å, those for the angles are 0−2°, and the dihedral angles change by 11° or less.

Solvation has a larger effect on the transition states. In the cyclic transition state, the S−O_{ap} leaving group bond is shortened by 0.05 Å, but the S−OH bond is lengthened; i.e., its value is 3.11 Å versus 2.96 Å in the gas phase. Also, the oxygen moiety of the hydroxy group is no longer directed toward the aliphatic hydrogens; the O(hydroxyl)−H(methylene) distance is 4.7 Å in solution versus 2.8 Å in the gas phase. While the OH hydrogen points away from the equatorial oxygen in the gas phase, the two interact in the TSC solution structure. This leads to a transition state geometry closer to an "in-line" approach: the O_{ap}−S−O_H angle is 138.70° for the cyclic transition state in the gas phase and 162.8° in solution (see Table 1). In the acyclic transition state, the S−O_{ap} distance decreases slightly (by 0.01 Å), and the S−OH bond length decreases significantly (from 2.978 Å in the gas phase to 2.635 Å in solution). The O_{ap}−S−O_H angle is 172.6° for the acyclic transition state in the gas phase and 174.5° in solution.

The geometry of attack by OH^- is thus much closer to in-line for the gas-phase acyclic reaction than for the cyclic case, and, at the transition states, the reaction coordinate is dominated by the elongation of the S−OH bond for the acyclic sulfate, while for the cyclic case, the elongation of the S−OH bond is coupled to the deformation of the O_{ap}−S−O_H angle. These differences in the nature of the reaction coordinate in the gas phase explains the different structural effects of solvation on the cyclic and acyclic transition states. The results of the SCI-PCM calculations have been confirmed by a two-dimensional mapping of the potential energy surface as a function of S−OH and O_{ap}−S−O_H (Lopez, X.; et al., to be published).

The gas-phase structures of the ion−molecule complexes IMC and IMAC were not reoptimized with the B3LYP(SCIPCM)/6-31+G* model. Since they are significantly destabilized by solvation, the gas-phase structure is not a good starting point for optimization in solution. For the cyclic ES−OH complex, several partial optimizations at the HF/6-31+G* level were made with the constrained S−OH distances (the S−OH distance was varied from 5 to 10 Å in steps of 0.5 Å). The gas-phase complexes were then solvated using the Poisson−Boltzmann method with the Mulliken charges obtained at each geometry (see section 2.2). At an S−OH distance of 9 Å, the solvated complex is only 1.5 kcal/mol lower in energy than the solvated reactants. Such a low-energy, long-range complex, if it exists, is not expected to influence the reaction kinetics.

3.2.b. Energetics. Table 3a lists free energies in solution of the various stationary points relative to the solvated reactants; the free energies of solvation calculated with the various methods are given in Table 3b. Six values of the solvation free energy are calculated for each stationary point. Three of those correspond to the solvation of the gas-phase B3LYP/6-31+G* structures using Poisson−Boltzmann, PCM, and SCI-PCM methods, respectively. The three other values are determined from the structures obtained by optimization in solution using the SCI-PCM method at the B3LYP(SCI-PCM)/6-31+G* level and calculating the solvation free energy for these structures with the Poisson−Boltzmann, PCM, and SCI-PCM methods. The single-point HF(PCM)/6-31+G* calculation were made to determine a more meaningful energy of solvation than that resulting from the SCI-PCM model. Comparison of the solvation corrections obtained for the two sets of structures makes it possible to separate the effect of the solvent on the energy of the gas-phase B3LYP/6-31+G* structures from the combined structural and energetic effect of solvation.

(36) Cameron, D. R.; Thatcher, G. R. J. *J. Org. Chem.* **1996**, *61*, 5986.

Table 3. (a) Relative Gibbs Free Energies of Stationary Points in Solution, Calculated at the B3LYP/6-31+G* Gas-Phase and SCIPCM Geometries, Using Solvation Energies from the Poisson−Boltzmann Calculations (PB),[a] from the SCI-PCM Calculations (SCI-PCM), and from the PCM HF/6-31+G* Calculations (PCM), and (b) Solvation Free Energies, in kcal/mol[a]

(a) Relative Gibbs Free Energies

		ΔG_{aq}					
		PB		SCI-PCM		PCM	
structure	ΔG_{gas}	gas	SCI-PCM	gas	SCI-PCM	gas	SCI-PCM
			Cyclic				
IMC	−28.2	10.7		3.1			
TSC	4.8	31.9	15.2 (24.1)	22.7	13.9	19.8	17.2
IC	−29.0	5.4	0.9 (4.7)	−7.0	−7.3	6.2	5.1
			Acyclic				
IMAC	−22.8	18.3		5.3			
TSAC	−5.5	29.6	24.4 (28.9)	14.8	14.31	21.4	23.0
IAC	−16.1	19.9	16.6 (19.3)	7.6	7.02	21.6	18.6
IAC′	−15.9	17.9		8.0			
IAC″	−15.6	19.0		9.0			

(b) Solvation Free Energies

	PB		SCI-PCM		PCM	
structure	gas	SCI-PCM	gas	SCI-PCM	gas	SCI-PCM
OH	−95.1	−95.1 (−95.0)	−65.6	−65.6	−93.8	−92.5
			Cyclic			
ES	−8.2	−11.9 (−8.7)	−7.9	−9.0	−15.3	−14.6
IMC	−64.4		−42.3			
TSC	−76.2	−95.8 (−84.4)	−55.4	−68.1	−84.5	−94.7
IC	−68.9	−77.1 (−70.0)	−51.6	−53.2	−73.9	−73.0
			Acyclic			
DMS	−8.5	−11.2 (−9.0)	−6.5	−6.9	−11.5	−11.1
IMAC	−62.5		−44.0			
TSAC	−68.5	−77.7 (−69.7)	−51.8	−52.7	−78.4	−75.1
IAC	−67.6	−73.5 (−68.7)	−48.3	−49.7	−67.6	−68.9
IAC′	−69.8		−48.2			
IAC″	−69.0		−47.5			

[a] Values in parentheses correspond to the solvation energies from Poisson−Boltzmann calculations using gas-phase B3LYP/6-31+G* Mulliken charges. The other values correspond to the B3LYP(SCI-PCM)/6-31+G* charges. [b] For the PB calculations with SCI-PCM geometries, two sets of Mulliken charges were considered, those obtained from the B3LYP(SCI-PCM)/6-31+G* wave function and those obtained from the B3LYP/6-31+G* one (in parentheses).

From Table 3b, the individual values of the solvation free energies vary significantly for the different methods. As expected (see section 2.2), the Poisson−Boltzmann calculations and the PCM calculations show corresponding behavior, while the SCI-PCM solvation corrections are significantly smaller. Qualitatively, the effects of solvation on the cyclic and acyclic stationary points are similar. The transition states and intermediates are significantly destabilized in solution; the ion−molecule complex is also strongly destabilized by solvation, as mentioned in section 3.2a. From Table 3b, it is evident that the structural change occurring in solution is accompanied by a large increase in the solvation free energy of the cyclic transition state, while the effect on the acyclic species is much smaller.

Table 4. Mulliken Atomic Charges at B3LYP/6-31+G* (Gas) and B3LYP(SCI−PCM)/6-31+G* (Solution) for (a) the Cyclic Reaction and (b) the Acyclic Reaction[a]

	reactants		transition-state		intermediate	
atom	gas	solution	gas	solution	gas	solution
			(a) Cyclic Reaction			
S	1.781	1.821	1.670	1.912	1.704	1.862
O1	−0.547	−0.592	−0.618	−0.605	−0.676	−0.771
O2	−0.547	−0.592	−0.527	−0.595	−0.743	−0.803
Oap	−0.544	−0.562	−0.577	−0.610	−0.525	−0.600
Cap	−0.260	−0.271	−0.229	−0.261	−0.260	−0.205
H_{Cap}	0.232	0.268	0.191	0.236	0.169	0.174
H_{Cap}	0.232	0.259	0.177	0.246	0.142	0.183
Oeq	−0.544	−0.562	−0.617	−0.636	−0.596	−0.639
Ceq	−0.260	−0.271	−0.358	−0.264	−0.171	−0.187
H_{Ceq}	0.232	0.268	0.275	0.246	0.149	0.193
H_{Ceq}	0.232	0.259	0.187	0.239	0.160	0.186
O_{hyd}	−1.334	−1.331	−1.266	−1.269	−0.795	−0.868
H_{hyd}	0.334	0.331	0.366	0.362	0.441	0.474
			(b) Acyclic Reaction			
S	1.827	1.858	1.793	1.948	1.794	1.940
O1	−0.609	−0.654	−0.641	−0.649	−0.790	−0.841
O2	−0.609	−0.654	−0.555	−0.729	−0.686	−0.764
Oap	−0.546	−0.553	−0.575	−0.624	−0.567	−0.633
Cap	−0.443	−0.457	−0.451	−0.438	−0.416	−0.390
H_{Cap}	0.222	0.243	0.175	0.209	0.139	0.164
H_{Cap}	0.242	0.248	0.215	0.216	0.182	0.177
H_{Cap}	0.219	0.245	0.201	0.213	0.164	0.174
Oeq	−0.546	−0.553	−0.569	−0.585	−0.512	−0.571
Ceq	−0.443	−0.457	−0.494	−0.427	−0.444	−0.414
H_{Ceq}	0.222	0.243	0.156	0.199	0.156	0.199
H_{Ceq}	0.242	0.248	0.380	0.297	0.219	0.208
H_{Ceq}	0.219	0.245	0.174	0.196	0.203	0.206
O_{hyd}	−1.334	−1.331	−1.193	−1.197	−0.881	−0.912
H_{hyd}	0.334	0.331	0.387	0.371	0.439	0.459

[a] For the acyclic system, only the data for the IAC intermediate are shown.

Table 4lists the gas phase and solution Mulliken charges[37] for the cyclic and acyclic reactions. The values for reactants, transition states, and intermediates are shown. In general, larger charges are obtained in solution than in the gas phase, indicative of the polarization introduced by the solvation. The largest enhancements of atomic charges in solution are observed for sulfur and the oxygen atoms. The amount of negative charge transferred from the hydroxyl group to the sulfate is less in solution than in the gas phase. The hydroxy group at the gas-phase transition states shows a Mulliken charge of −0.900 and −0.806 e^- in the cyclic and acyclic cases, respectively; in solution, these values are −0.907 and −0.880 e^-. The same is true for the intermediates. The origin of this effect is that a larger concentration of charge on a single exposed group leads to a larger solvation free energy, since the latter depends approximately on the square of the charge, as in the Born model.

The overall effect of solvation on the reaction profile is similar to what has been observed in other studies of nucleophilic attack by an ion on a neutral dipolar molecule.[38,39] Solvation favors the separate reactants over the ion−molecule complex, the transition state, and the intermediates. The net result is an increased solvent-induced barrier to hydrolysis relative to the reactants. The activation barrier calculated for the hydrolysis is 17.2 kcal/mol for the cyclic sulfate (PCM results, cf. Table 3a)

(37) Mulliken atomic charges have to be analyzed with care, especially when diffuse functions are contained in the basis set. Although the value of the atomic charge can differ substantially with the method and the basis set used, the overall trends, in general, are similar.

(38) Bash, P. A.; Field, M. J.; Karplus, M. *J. Am. Chem. Soc.* **1987**, *109*, 8092−8094.

(39) Chandrasekhar, J.; Smith, S. F.; Jorgensen, W. L. *J. Am. Chem. Soc.* **1985**, *107*, 154.

and 23 kcal/mol for the acyclic sulfate. Table 3a shows the range of values obtained with the different methods. Overall, the various species behave consistently, so that the calculated barriers are similar even though the individual solvation energies vary. (The exception is the SCI-PCM barrier for the acyclic system, which is too low (14.8 kcal/mol) with respect to the Poisson−Boltzmann (PB) and PCM values of 20−24 kcal/mol. As explained in the Methods section, the largest error in computing solvation free energies is expected for the SCI-PCM method, which gives a solvation free energy for OH^- which is only about two-thirds of the experimental value.) The corresponding experimental values for the activation energy barrier are 7.9 kcal/mol for the cyclic systems and 17.8−20.2 kcal/mol for the acyclic system.[6,7] The calculated barriers in solution are thus in reasonable agreement with experimental values for the acyclic sulfate and somewhat too large for the cyclic sulfate. Overall, the agreement between calculated and experimental activation barriers is similar to what has been observed in other studies using solvation corrections of this type.[40] In particular, the values presented in Table 3a use the solute entropy contributions from the gas phase (cf. Table 2a) without correction for changes in entropy upon solvation. This simplified description of the entropy contribution has been adopted because of the computational cost of calculating vibrational modes with a solvation correction. It has been argued[40] that the complexes formed in solution are generally "floppier" than those formed in the gas phase, so that the entropy loss should be smaller in solution. This would, in effect, reduce the activation free energy from the values presented in Table 3a, and the effect should be more pronounced for the cyclic sulfate, which occurs at a larger S−OH distance (3.11 Å) than the acyclic one (S−OH = 2.65 Å). Additional calculations are required to verify the conjecture.

The barriers computed by the PB and PCM methods using the SCI-PCM structures show that the hydrolysis of the cyclic sulfate is favored by 6 kcal/mol over that of the acyclic sulfate. This value is in approximate agreement with the experimentally observed rate acceleration of 10^7 for the cyclic sulfate, which corresponds to a difference in the activation free energies of about 10 kcal/mol. It is important to note that the path for the reaction in solution is not identical to that in the gas phase. This is true for the overall path and for the stationary points, so that structural optimization plays an essential role in obtaining meaningful free energies in solution; i.e., both structural and energetic effects of solvation contribute to the calculated rate acceleration. As can be seen from Table 3a, the relative stabilities of the pentacovalent intermediates are not affected by solvation and remain around 12−14 kcal/mol, favoring the cyclic compound, as found by Thatcher and Cameron.[16] Their mechanistic interpretation based on the behavior of the pentacovalent intermediates is therefore very different from ours, which is based on the actual transition states.

4. Comparison with the Hydrolysis of Basic Phosphates

The reaction profiles presented here for the basic hydrolysis of dimethyl (DMS) and ethylene (ES) sulfate in the gas phase and in solution can usefully be compared with those for the corresponding reaction of the isoelectronic dimethyl (DMP^-) and ethylene (EP^-) phosphate. Even though DMS and ES are isoelectronic with DMP^- and EP^-, an important difference is that they are neutral, while DMP^- and EP^- have a charge of −1, as described earlier. This has important consequences on the reaction profile of both species in the gas phase and in solution. Some aspects of the basic hydrolyis of the neutral sulfates are closer to what has been reported for the corresponding reaction of neutral phosphates, such as methyl ethylene phosphate (MEP).[41]

The overall shape of the reaction profile for the basic hydrolysis of DMS and ES in the gas phase is dramatically different from that of DMP^- and EP^-. In the hydrolysis of DMP^- and EP^-, there is no ion−molecule complex, and the reaction proceeds directly from the reactants to the transition state. This transition state is much higher in energy (approximately 95 kcal/mol) than what is observed for the sulfates (approximately 5 kcal/mol for ES, and −5.0 kcal/mol for DMS) due to the Coulombic repulsion between the two ionic reactants, and the P- - -O(H) distances found in the transition states are significantly shorter (namely, 2.2 and 2.6 Å, respectively, for DMP^- and EP^- at the B3LYP/6-31+G* level of theory versus 2.6 and 3.1 Å for DMS and ES). Pentacovalent phosphorane intermediates either do not exist or are only marginally stable.[10,11,42]

The reaction paths for the base-catalyzed hydrolysis of the neutral methyl ethylene phosphate (MEP)[41] and the hydrolysis by water rather than by a hydroxide ion of DMP^- and EP^- are much closer to those of the sulfates (Lopez, X.; et al., unpublished data). For methyl ethylene phosphate, there is a negative barrier of −4.3 kcal/mol, an early transition state with a P−OH distance of 2.9 Å, and stable phosphorane intermediates. Ion−molecule complexes are found in the hydrolysis of MEP as well, though they have not been fully characterized. [14]

The overall effects of solvation on the hydrolysis reaction are also qualitatively different for DMP, ES and DMP^-, EP^-. The barrier for the hydrolysis of DMS and ES with respect to the reactants is significantly increased by the presence of solvent, and solvation favors a more in-line approach of the hydroxide anion than in the gas phase. This in-line approach leads to greater stabilization of the hydroxy moiety by the solvent, which balances the lack of OH aliphatic hydrogen interactions (cf. section 3.2.b). The barrier for the reaction of DMS (ES) with respect to reactants is −5.5 (4.8) kcal/mol in the gas phase and 23.0 (17.2) kcal/mol in solution. The ion−dipole complex is strongly destabilized in solution. The energy barriers for the phosphates are very high in the gas phase, and solvation lowers the barriers by a large amount; i.e., the calculated activation free energies in solution are 37.7 and 29.6 kcal/mol for DMP^- and EP^-, respectively, relative to the gas-phase value of 95 kcal/mol. Moreover, solvation has only a very small effect on the transition-state geometries (Lopez, X.; et al., unpublished data) because the hydrolysis of phosphates proceeds by in-line attack without formation of an ion−molecule complex in the gas phase, as well as in solution. Again, the solvent effect for the base-catalyzed hydrolysis of the neutral methyl ethylene phosphate (MEP)[41] is much closer to that found for the sulfates, and solvent increases the barrier for the hydrolysis by 30 kcal/mol with respect to the gas-phase values.

Despite the above difference in the hydrolysis reaction between the sulfates DMS, ES and the phosphates DMP^-, EP^-, the measured relative reactivity of the cyclic sulfate versus that of the acyclic sulfate is essentially the same as that for the corresponding phosphates; i.e., for both the sulfates and the phosphates, the cyclic esters hydrolyze 10^6−10^8 times faster than the acyclic esters. In the gas phase, the ab initio calculations for the sulfate esters yield a destabilization of the cyclic versus acyclic reactant due to ring strain effects of about 5 kcal/mol,

(40) Florian, J.; Warshel, A. *J. Phys. Chem. B.* **1998**, *102*, 719−734.

(41) Tole, P.; Lim, C. *J. Phys. Chem.* **1993**, *97*, 6212.

(42) Uchimaru, T.; Tanabe, K.; Nishikawa, S.; Taira, K. *J. Am. Chem. Soc.* **1991**, *113*, 4351−4353.

in good agreement with the estimated value of 4 kcal/mol in the phosphates. In both the sulfate and the phosphate, this destabilization of the cyclic reactant in the gas phase does not lead to a reduced energy barrier in the transition state for hydrolysis. The absence of any effect on the activation barrier is due to several factors. First, the transition state for the hydrolysis of sulfates occurs early on the reaction path (at a S−OH distance of 3 Å), and little relief of ring strain has occurred at this point. Second, the acyclic reactant has rotational freedom around the S−O equatorial bond, which is not available to the cyclic reactant. This allows the acyclic transition state to be stabilized by an intramolecular interaction between the incoming hydroxyl group and an aliphatic hydrogen from a methyl group. No such interaction can stabilize the cyclic transition state, so that the barrier to hydrolysis is actually higher for the cyclic sulfate than it is for the acyclic sulfate in the gas phase. In the case of the corresponding dimethyl and ethylene phosphates, corresponding intramolecular stabilization effects of the acyclic compound were observed, and the calculated gas-phase activation barriers were similar for the cyclic and acyclic compounds.[10,11]

When the effect of solvation on the transition state is taken into account, the activation barrier for the hydrolysis of the cyclic sulfate is lower than that for the acyclic sulfate, in agreement with experimental observations. The intramolecular stabilization of the acyclic compound is no longer competitive with respect to intermolecular stabilization of the incoming OH^- by the solvent. As in the case of the phosphate esters, the cyclic transition state is better solvated than the acyclic one. This arises from the longer S−O(H) distance in solution and from the presence of the ring, which restricts the position of the equatorial $-OCH_2$ group. In the acyclic system, the equatorial methoxy group contributes significantly to the shielding of the incoming OH^- from the solvent. Thus, for the alkaline hydrolysis of the phosphate and sulfate esters, solvation favors the cyclic transition state, and this arises from a better solvation of the OH^- moiety in both cases.

5. Conclusions

Gas-phase ab initio and solution calculations have been performed for the acyclic and cyclic sulfate reactions to complement earlier work on phosphates. One of the essential facts of basic sulfate and phosphate ester hydrolysis is the very large rate acceleration of the cyclic versus the acyclic reactants. The high-level ab initio study performed here of the sulfate hydrolysis reaction shows that this rate acceleration cannot be explained by the gas-phase free energy profiles. For the isoelectronic phosphate esters DMP^- and EP^-, it was also found that the gas-phase free energy profiles could not explain the enhanced reactivity of the cyclic phosphate with respect to the acyclic one.[10−12]

Theoretical estimates of solvation effects show that the cyclic transiton states are better solvated than the acyclic ones. This arises essentially from a better solvation of the OH^- moiety of the cyclic compounds. Thus, consideration of the free energy profile in solution explains the enhanced reactivity of the cyclic compounds over the acyclic ones. The behavior of the sulfate and phosphate esters is similar in this respect, even though the difference in charges lead to markedly different energetics for the two types of compounds. Our conclusion differs from that of Thatcher and Cameron, who argued in a recent paper on the hydrolysis of sulfates that "there is a discrepancy between the results for cyclic sulfate and phosphate systems which may be explained if the causes of the similar rate acceleration observed in hydrolysis of five-membered cyclic phosphates and sulfates are entirely different".[16] As already mentioned, this conclusion was based on a comparison between the energetics and solvation of the reaction intermediates. Consideration of the transition states shows that the results for sulfate esters are coherent with those for the phosphate esters; i.e., for both systems, in contrast to the view held for 30 years, solvation rather than steric strain makes the dominant contribution to the difference in hydrolysis rates between the cyclic and acyclic esters.

Acknowledgment. The laboratory is supported in part by the CNRS (ISIS-UPRES A 7006), by the Ministère de l'Education Nationale, and by a grant from the Association pour la Recherche contre le Cancer (France). Work done at Harvard University was supported in part by a grant from the National Science Foundation (U.S.A.). X.L. thanks the Spanish Ministerio de Educacion y Cultura (MEC) for a grant. We also thank the Institut de Development et des Ressources en Informatique Scientifique (IDRIS) for computer time and assistance in this work.

Supporting Information Available: Table showing complete deformation analysis, including interaction energies for cyclic and acyclic sulfates and the deformation energy for the sulfate moiety (PDF). This material is available free of charge via the Internet at http://pubs.acs.org.

JA984193Q